OPTIMIZED FORCE ALLOCATION

A General Approach to Control and to Investigate the Motion of Over-Actuated Vehicles

Christian Knobel * **Alfred Pruckner** *
Tilman Bünte **

* *BMW Group Research and Technology, 80788 Munich, Germany, christian.knobel@bmw.de*
** *German Aerospace Center (DLR), Institute of Robotics and Mechatronics, Oberpfaffenhofen, Germany*

Abstract: A general approach is introduced to allocate the forces acting on the center of gravity to the four wheels of a vehicle by using an inversion of vehicle dynamics and a non-linear optimization. This makes it possible to compare all useful configurations of actively and passively controlled influencing variables of vehicle dynamics (steering angles, brake/drive torques, wheel loads and camber angles), with and without actuator dynamics and to investigate the impact of actuator failures on vehicle dynamics.

Keywords: Force Allocation, Non-linear Optimization, Vehicle Dynamics, Global Chassis Control, Tyre Contact Patch, Adhesion Potential Utilization, Tyre Based Vehicle Dynamics Control

1. INTRODUCTION

Stabilizing vehicle dynamics by controlling the individual brake torques was introduced in 1995 and is now state of the art even in small road vehicles. The control of vertical dynamics, front and rear wheel steering angles as well as the active distribution of drive torque went already to series production, too. Because of the physical interdependencies between these systems, integration is needed to operate a vehicle with more than one of these systems [1]. In the last decades, many approaches focused on special configurations have been presented. In order to find a general approach for steering and brake/drive systems improving vehicle dynamics (Hattori *et al.*, 2002) presented the idea to use non-linear optimization. Instead of minimizing the error of the vehicle motion, (Ono *et al.*, 2004) and (Orend, 2004) introduced a minimization of the adhesion potential utilization of all tyres for a vehicle with individual brake/drive torque, single wheel steering and active suspension. (Andreasson and Bünte, 2005) linearized this approach and introduced constraints for different chassis configurations. To be able to investigate driving situations even if the vehicle is reaching the physical limit, the paper at hand complements the non-linear approach of minimizing the adhesion potential (Sec. 4), based on the inversion of vehicle and tyre model introduced in Sec. 2 and 3. All variables influencing the force transfer between the road and the vehicle through the tyre contact patches (TCP), i.e. steering angles $\boldsymbol{\delta} = \begin{bmatrix}\delta_1 & \delta_2 & \delta_3 & \delta_4\end{bmatrix}^T$, brake/drive torques $\boldsymbol{M} = \begin{bmatrix}M_1 & M_2 & M_3 & M_4\end{bmatrix}^T$, wheel loads $\boldsymbol{F_z} = \begin{bmatrix}F_{z1} & F_{z2} & F_{z3} & F_{z4}\end{bmatrix}^T$ and even camber angles

[1] cf. (Andreasson *et al.*, 2006) for a detailed classification of systems for vehicle motion control.

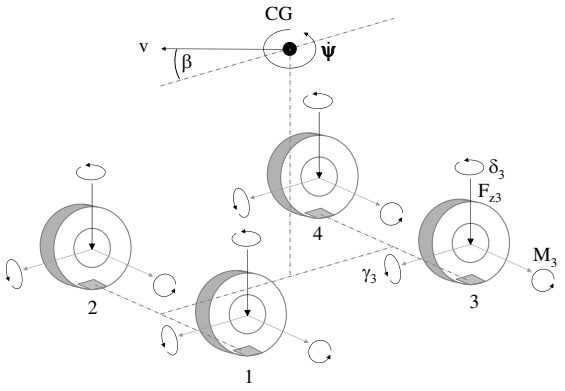

Fig. 1. Plane Vehicle Model with Influencing Variables and Vehicle Motion $\boldsymbol{y}$

$\boldsymbol{\gamma} = \begin{bmatrix}\gamma_1 & \gamma_2 & \gamma_3 & \gamma_4\end{bmatrix}^T$ (Sec. 5) are considered (cf. Fig. 1). Finally, simulation results are presented in Sec. 6.

2. VEHICLE MODEL

Neglecting the relative motion between the center of gravity (CG) and the wheels, the vehicle motion $\boldsymbol{y} = \begin{bmatrix}\dot{\psi} & \beta & v\end{bmatrix}^T$ can be described by the yaw rate $\boldsymbol{\dot{\psi}}$, the body side slip angle $\boldsymbol{\beta}$ and the velocity $\boldsymbol{v}$ of the vehicle's CG, which leads to a plane description of the vehicle's motion (cf. e.g. (Orend, 2004)). To fulfill this motion, a unique vector of forces and torques, respectively

$$\boldsymbol{u} = \begin{bmatrix}M_z\\F_x\\F_y\end{bmatrix} = \underbrace{\begin{bmatrix}\Theta\ddot{\psi}\\ m(\dot{v}\cos\beta - v(\dot{\psi}+\dot{\beta})\sin\beta)\\ m(\dot{v}\sin\beta + v(\dot{\psi}+\dot{\beta})\cos\beta)\end{bmatrix}}_{\boldsymbol{d(y,\dot{y})}} \quad (1)$$

acting on the CG is necessary. This relation represents nothing but the inversion of a state space system where the (angular) velocities

$$\boldsymbol{x} = \begin{bmatrix}\dot{\psi}\\ v_x\\ v_y\end{bmatrix} = \begin{bmatrix}\dot{\psi}\\ v\cos\beta\\ v\sin\beta\end{bmatrix} \quad (2)$$

are chosen as states. The state space system can be written as:

$$\dot{\boldsymbol{x}} = \underbrace{\begin{bmatrix}0\\ v_y\dot{\psi}\\ -v_x\dot{\psi}\end{bmatrix}}_{\boldsymbol{f(x)}} + \underbrace{\begin{bmatrix}\frac{1}{\Theta} & 0 & 0\\ 0 & \frac{1}{m} & 0\\ 0 & 0 & \frac{1}{m}\end{bmatrix}}_{\boldsymbol{B}}\boldsymbol{u}\ ,\ \boldsymbol{y} = \underbrace{\begin{bmatrix}\dot{\psi}\\ \arctan\frac{v_y}{v_x}\\ \sqrt{v_x^2+v_y^2}\end{bmatrix}}_{\boldsymbol{h(x)}} \quad (3)$$

According to Fig. 2 the geometric relations between $\boldsymbol{u}$ and

$$\boldsymbol{F} = \begin{bmatrix}F_{x1} & F_{x2} & F_{x3} & F_{x4} & F_{y1} & F_{y2} & F_{y3} & F_{y4}\end{bmatrix}^T \quad (4)$$

are summarized by $\boldsymbol{G}$.

$$\boldsymbol{u} = \underbrace{\begin{bmatrix}-\frac{s}{2} & \frac{s}{2} & -\frac{s}{2} & \frac{s}{2} & l_f & l_f & l_r & l_r\\ 1 & 1 & 1 & 1 & 0 & 0 & 0 & 0\\ 0 & 0 & 0 & 0 & 1 & 1 & 1 & 1\end{bmatrix}}_{\boldsymbol{G}}\boldsymbol{F} \quad (5)$$

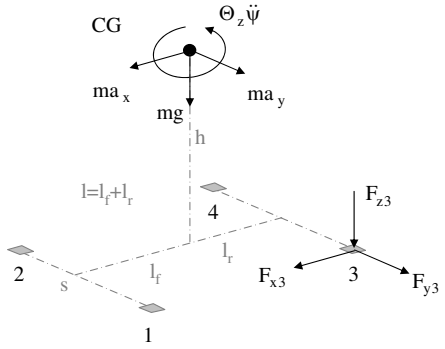

Fig. 2. Geometric and Kinetic Relations

Although the relative motion of the CG to the TCPs is neglected, the wheel load distribution

$$\underbrace{\begin{bmatrix}mg\\0\\0\end{bmatrix} + \begin{bmatrix}0&0&0\\0&h&0\\0&0&h\end{bmatrix}\boldsymbol{u}}_{\boldsymbol{u_z}} = \underbrace{\begin{bmatrix}1 & 1 & 1 & 1\\ -l_f & -l_f & l_r & l_r\\ -\frac{s}{2} & \frac{s}{2} & -\frac{s}{2} & \frac{s}{2}\end{bmatrix}}_{\boldsymbol{V}}\boldsymbol{F_z} \quad (6)$$

is considered.

For the conventional tyre the analytic Magic Formula (Pacejka, 2002) is used as model, which calculates first the pure forces

$$\begin{aligned}F'_{xio} &= D\sin\left(C\arctan\left(B\kappa - E(B\kappa - \arctan B\kappa)\right)\right)\\ F'_{yio} &= D\sin\left(C\arctan\left(B\alpha - E(B\alpha - \arctan B\alpha)\right)\right)\end{aligned} \quad (7)$$

$i \in \{1\dots4\}$ designated with $'$ to indicate the respect to the wheel coordinate system. Secondly,

$$\begin{aligned}F'_{xi} &= F'_{xio}\cos\left(C\arctan\left(B\alpha - E(B\alpha - \arctan B\alpha)\right)\right)\\ F'_{yi} &= F'_{yio}\cos\left(C\arctan\left(B\kappa - E(B\kappa - \arctan B\kappa)\right)\right)\end{aligned} \quad (8)$$

the interdependence between the longitudinal and lateral tyre forces is considered where the peak factors $D(F_z,\gamma)$, the shape factors C, the stiffness factors $B(F_z,\gamma)$ and the curvature factors $E(F_z,\gamma)$ are different for (7), (8) and for longitudinal and lateral direction, respectively. The matrix $\boldsymbol{T}(\boldsymbol{\delta})$

$$\boldsymbol{F} = \boldsymbol{T}(\boldsymbol{\delta})\boldsymbol{F'} \quad (9)$$

transforms the forces $\boldsymbol{F'}$ from the wheel coordinate system into the vehicle coordinate system. Considering the effective rolling radius r_e and the velocities in the TCPs [2], the relation of the forces F' to the influencing variables [3] is given by

$$\boldsymbol{M} = \frac{\boldsymbol{F'_x}}{r_e}\ ,\ \boldsymbol{\alpha} = -\arctan\left(\frac{\boldsymbol{v_x}\sin\boldsymbol{\delta} + \boldsymbol{v_y}\cos\boldsymbol{\delta}}{\boldsymbol{v_x}\cos\boldsymbol{\delta} - \boldsymbol{v_y}\sin\boldsymbol{\delta}}\right). \quad (10)$$

By combining (5), (3), (6), (9) and (8) a vehicle model is created where the influencing variables ($\boldsymbol{\delta}$, $\boldsymbol{M}$, $\boldsymbol{\gamma}$ and $\boldsymbol{F_z}$) are the inputs and the outputs are the components of the plane vehicle motion

[2] $\boldsymbol{v} = \begin{bmatrix}v_{x1} & v_{x2} & v_{x3} & v_{x4} & v_{y1} & v_{y2} & v_{y3} & v_{y4}\end{bmatrix}^T = (\boldsymbol{x}^T\boldsymbol{G})^T$.

[3] wheel dynamics are neglected.

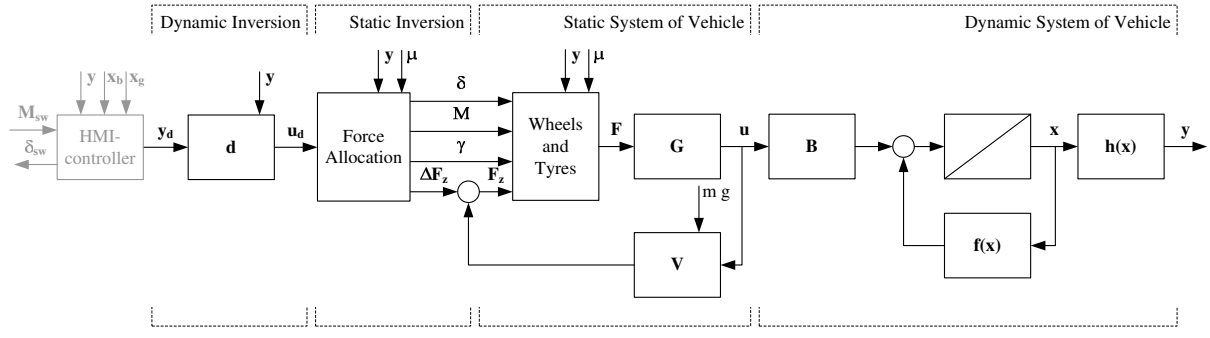

Fig. 3. Considered Vehicle Model and its Inversion

$\boldsymbol{y}$. This model consists of a static part, which comprises the static tyre model, $\boldsymbol{G}$ and $\boldsymbol{V}$, and a dynamic part represented by $\boldsymbol{B}$, $\boldsymbol{h(x)}$ and $\boldsymbol{f(x)}$ (cf. right part of Fig. 3).

3. MODEL INVERSION

Inversion is state of the art for motion control of military and commercial aircraft (Balas, 2003). Instead of controlling the behavior of control surfaces (e.g. rudder, aileron), the pilot controls the motion degrees of freedom of the aircraft directly. With the introduction of Active Front Steering (AFS), where the driver is not longer controlling the angles of the front wheels directly, this trend has started for vehicles as well. For stability control systems even today, the driver's input, consisting of steering wheel angle δ_{SW} or torque M_{SW} and the pedal positions x_g and x_b, is converted to a desired plane vehicle motion (e.g. $\boldsymbol{y_d}$), which is the reason why the paper at hand assumes $\boldsymbol{y_d}$ and it's derivative as the driver's input. Converting M_{SW}, x_g and x_b to $\boldsymbol{y}$ and providing an adequate haptic feedback are assumed to be tasks for an HMI controller. [4]

Inverting the introduced model (cf. Fig. 3) leads to the following difficulties: While the inversion of the dynamic system is already represented by (1), the inversion of $\boldsymbol{G}$ is under-determined and leads to a five dimensional region in the eight dimensional parameter space for which the desired vehicle motion $\boldsymbol{y_d}$ is fulfilled. The inversion of $\boldsymbol{V}$ is under-determined as well, which leads to another free parameter ΔF_z. [5] This six dimensional region of free parameters defines the freedom of any optimization improving the distribution of the forces while fulfilling the desired vehicle motion $\boldsymbol{y_d}$. In a conventional vehicle the degree of over-actuation [6] restricts this region. The inversion of the tyre model (7) is not strictly monotonic which makes an inversion in the entire scope impossible. Nevertheless, it is possible to invert only the stable (i.e. monotonic) area of (7) until the maximum is reached. Even if it is impossible to prevent operation in the unstable area for every situation [7], the controller introduced in this work does not use this unstable area (cf. Sec. 4). To complete the inversion, the two major effects of interdependence between the longitudinal and the lateral force are inverted as well. First, the interdependence between force and stiffness is inverted by complementing a force dependence to the stiffness factor B

$$B'_{x,y\,c} = B'_{x,y\,p}\,\cos\left(\arctan\left|\frac{F'^{3}_{y,x}\,F'^{2}_{x,y}}{b_{x,y}}\right|\right) \tag{11}$$

where b_x and b_y are coefficients. The limitation of the absolute value of the force comprising longitudinal and lateral force is the second interdependence. It is approximated by an elliptic relation. The norm of this elliptic relation

$$\eta_i^2 = \left(\frac{F_{xi}}{F_{xi\,max}}\right)^2 + \left(\frac{F_{yi}}{F_{yi\,max}}\right)^2 \tag{12}$$

represents the adhesion potential utilization η_i ($0 \le \eta_i \le 1$) for the each tyre $i \in \{1 \dots 4\}$. It is zero as long as no plane force is applied and one if the maximum force is applied. With the nominal wheel load F_{z0} and the road friction coefficients μ_i ($\boldsymbol{\mu} = \begin{bmatrix}\mu_1 & \mu_2 & \mu_3 & \mu_4\end{bmatrix}^T$) the maximum force

$$F'_{x,y\,i\,max} = \mu_i F_{zi} k_{x,y\,i}\left(1 + l_{x,y}\frac{F_{zi} - F_{z0}}{F_{z0}}\right) \tag{13}$$

can be described for longitudinal and lateral direction (cf. (Pacejka, 2002)). Both parameters $k_{y\,i}$ and $k_{x\,i}$ are depending on the actual camber (cf. Sec. 5). Assuming the coefficients l_x and l_y for the degressive behavior to be the same, (12) can be simplified to

$$\eta_i^2 = \frac{1}{(F'_{xi\,max})^2}\left(\left(\frac{F'_{xi}}{k_{x\,i}(\gamma_i)}\right)^2 + \left(\frac{F'_{yi}}{k_{y\,i}(\gamma_i)}\right)^2\right). \tag{14}$$

[4] cf. (Huang, 2004) for suggested HMI strategies and driver-vehicle control loop investigations.

[5] $\boldsymbol{u_z} = \boldsymbol{V F_z} + \boldsymbol{\Delta F_z}$ needs to be fulfilled e.g. $\boldsymbol{\Delta F_z} = \begin{bmatrix}1 & -1 & -1 & 1\end{bmatrix}^T \Delta F_z$

[6] cf. (Valášek, 2003) for definition and examples.

[7] e.g. sudden reduction of road friction coefficient μ while driving close to the adhesion limit.

Summarizing these effects the inverse tyre model

$$\kappa_i, \alpha_i = \tan\left(\frac{1}{C'_{x,y}} \arcsin \eta_i\right) \frac{F'_{x,y\,i}}{F'_{xi\,max} B'_{x,y\,c}} \quad (15)$$

describes the inversion of the tyre characteristics and is valid only for the stable area of the tyre.

4. OPTIMIZED FORCE ALLOCATION

The inversion of the static system leads to a six dimensional region of parameters which represents the freedom for any improvement of the distribution. Minimizing the error between $\boldsymbol{y_d}$ and $\boldsymbol{y}$ as presented in (Hattori *et al.*, 2002) is a robust objective which is reasonable even if the physical limit of the tyre/road contact is reached. This approach is also found in motion control of aircraft and is called *error minimization problem* (Bodson, 2002). Nevertheless, to improve the force allocation, minimizing the adhesion potential utilization η_i

$$\min_{\boldsymbol{\xi}} \max_{\boldsymbol{\eta}} \eta_i \quad (16)$$

as introduced in (Ono *et al.*, 2004) and (Orend, 2004) represents a feasible and convex (Orend, 2005) optimization objective. Since the physical driving limit of the vehicle is reached when two of one axle or more η_i are reaching one, it is desirable to minimize the maximum η_i which leads to a leveling of all four η_i. This prevents instability as long as possible. Even if the conditions are different, a similar approach for motion control of aircraft is introduced by (Bodson, 2002) and is called *control minimization problem*. However, this approach is only reasonable, as long as the desired motion is feasible. To be able to handle also driving situations reaching the physical limit while minimizing the control action, the approaches of error minimization and control minimization are combined in the paper at hand.

Reasonable as optimization parameters are either forces $\boldsymbol{\xi_f} = \begin{bmatrix}\boldsymbol{F}^T & \Delta F_z\end{bmatrix}^T$ representing the six dimensional region of free parameters directly or influencing variables $\boldsymbol{\xi_v} = \begin{bmatrix}\boldsymbol{\delta}^T & \boldsymbol{M}^T & \Delta F_z\end{bmatrix}^T$ representing the available actuators directly. As long as no constraints are used, it is reasonable to work with $\boldsymbol{\xi_f}$ which keeps the representation of the optimization objective as function of the optimization parameters simple. For this work however, $\boldsymbol{\xi_v}$ is used instead, because it allows a simpler way of implementing the necessary constraints for the intended comparisons. Since the chosen optimization objective (16) only takes care of the allocation of the force while fulfilling $\boldsymbol{y_d}$, it is only valid for a feasible (i.e. $\eta_i < 1$) desired motion $\boldsymbol{y_d}$. To be able to handle also driving situations where the driving limit is reached (i.e. $\eta_i = 1$), $\boldsymbol{y_d}$ needs to be adapted such that $\boldsymbol{u_d}$ is feasible. This is done by integrating a flat [8] stability controller into the optimization objective. The inversion (cf. (1)) is therefore complemented with a linear error part representing a proportional feedback [9]

$$\boldsymbol{u_d} = \boldsymbol{d}(\boldsymbol{y}, \boldsymbol{y_c}) \quad \text{where} \quad (17)$$

$$\boldsymbol{y_c} = \dot{\boldsymbol{y_d}} + \operatorname{diag}(\boldsymbol{p})(\boldsymbol{y_d} - \boldsymbol{y}) \quad (18)$$

with the proportional gain vector $\boldsymbol{p} = \begin{bmatrix}p_\psi & p_\beta & p_v\end{bmatrix}^T$. To guarantee feasibility a reduction vector $\boldsymbol{r}(\boldsymbol{\xi}) = \begin{bmatrix}r_\psi & r_\beta & r_v\end{bmatrix}^T$ is introduced. As long as $\boldsymbol{u_d}$ is feasible (i.e. $\eta < 1$) $\boldsymbol{r}$ equals $\boldsymbol{y_c}$. A pre-optimization generates starting values for (16) and is able to decrease $\boldsymbol{u_d}$ if $\boldsymbol{u_d}$ is physically impossible.

$$\min_{\boldsymbol{\xi}} (\boldsymbol{y_c} - \boldsymbol{r})^T \boldsymbol{W} (\boldsymbol{y_c} - \boldsymbol{r}) \quad (19)$$

$$\text{such that } \boldsymbol{u} = \boldsymbol{G}\boldsymbol{F} \text{ and } \eta_i \leq 1$$

where $\boldsymbol{W} = \operatorname{diag}\begin{bmatrix}w_\psi & w_\beta & w_v\end{bmatrix}^T$ represents the weight of the penalty.

Reduction of optimization parameters or constraints representing the setup of actuators, their dynamics and their failures are designed for investigation and comparison. To represent the available actuators the interdependencies of the influencing variables need to be described. [10] In this way all kind of steering (e.g. individual-, rack- or no-steering) and drive setups (e.g. individual, differentially distributed, no-drive) can be applied for the front and the rear axle while the brake setup is always assumed to be individually controllable. While the distribution of the wheel loads can be done either actively or passively (i.e. with or without controllable actuator), the camber angles are assumed to be directly, indirectly (e.g. controlling body roll φ) or passively controllable (cf. Sec. 5). The availability of actuators can be changed not only once but also while driving in order to investigate the impact of actuator failures on vehicle dynamics. This reconfigurable behavior is given by the possibility to change the number and type of constraints and optimization parameters of the optimization. How the available actuators for steering and drive need to be represented depends on the chosen optimization parameters (e.g. $\boldsymbol{\xi_f}$ or $\boldsymbol{\xi_v}$). If the forces $\boldsymbol{\xi_f}$ are used, the interdependencies of the influencing variables need to be converted to forces using the inversion of the tyre model introduced in Sec. 3. The consideration of actuator dynamics is represented by constraints for the optimization as well. The maximum velocity and acceleration is constrained by defining the area of valid solutions for the next optimization step in dependence to the actuator dynamics of the actual simulation step (cf. (Andreasson and Bünte, 2005)).

---

[8] cf. (Orend, 2005) for analysis

[9] The feedback is done without integral action i.e. the driver has to compensate for steady state errors.

[10] e.g. steering rod for rack steering i.e. $\delta_1 = \delta_2$.

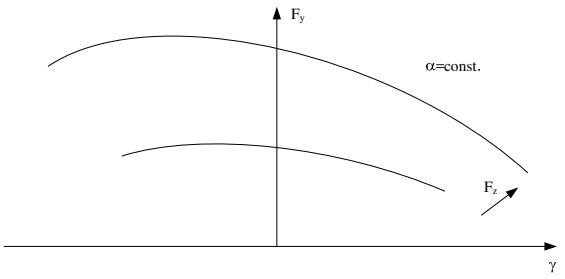

Fig. 4. Effect of Camber Angle γ on Lateral Tyre Force F_y while const. Tyre Side Slip Angle α

5. INFLUENCE OF CAMBER ANGLE

After the forces are distributed to the wheels considering to the optimization objective (16), the force transfer within the area of the TCPs needs to be investigated with respect to (16). This is influenced by the tyre parameters, the road surface, the wheel load F_{zi} and the camber angle γ_i. Since the free parameter ΔF_z of the wheel load affects the force allocation, it was already considered in Sec. 4. Even if the influence [11] of the camber angles are implicity considered in the force allocation cf. (13), $\boldsymbol{\gamma}$ was not used consciously as optimization parameter for (16). However, if $\boldsymbol{\gamma}$ is controllable it can be calculated independent from the allocation.

To be able to transfer the highest possible force, the area of the TCP needs to be maximized. In the situation of straight driving a camber angle greater than zero reduces this area independently from its direction. As soon as lateral force is applied the effect of the camber on the force depends on its direction. This can be explained with the deformation of the tyre belt or rather the TCP due to the acting lateral force. If the camber is counteracting this effect, the force increases until both effects in an equilibrium. If the camber is acting in the same direction, the lateral force decreases (cf. Fig. 4). Even if the intensity of camber influence depends on the specific tyre behavior [12], the influence in general is valid for all conventional tyres. The coefficient

$$k_{yi} = k_{yi0} + k_{yi1}\ \operatorname{sign} F_{yi} \left(\frac{F_{yi}}{F_{yN}} \right)^2 \gamma + k_{yi2}\gamma^2 \tag{20}$$

describes the camber influence on the lateral force. Since the influence of the camber is known, optimal camber

$$\gamma_i = c_1\ \operatorname{sign} F_{yi} \left(\frac{F_{yi}}{F_{yN}} \right)^2 \tag{21}$$

for every given lateral force can be derived from (20).

6. SIMULATION RESULTS

A vehicle controlling all influencing variables actively (active vehicle) is compared with a conventional vehicle where only the front rack steering system and the brakes are actively controllable by the force allocation. To allow an easy comparison a feasible maneuver (i.e. $\eta < 1$) is chosen to guarantee both vehicles can fulfill the desired motion $\boldsymbol{y_d}$ presented in Fig. 5. The speed $v = 100$km/h starts to reduce at 0.5s with $a_x = -2\mathrm{m}/s^2$ on wet road $\mu_i = 0.6$. At the same time the yawing corresponding to a single lane change starts. The influencing variables are acting on a multi-body model of an actual vehicle (cf. Fig. 6). For the active vehicle $\boldsymbol{\delta}$, $\boldsymbol{M}$ and $\boldsymbol{F_z}$ calculated by the optimization while the camber angles are calculated by (21). The camber for the conventional vehicle results from the roll angle φ, in consequence of parallel movement because of the single wheel suspension setup, the compression of the tyres, the suspension kinematics, and the lateral force acting on the TCP. The resulting adhesion potential utilizations η_i are presented in Fig. 7. All η_i of the active vehicle are leveled to the same value. This is impossible if the optimization can only use the brakes and the active front rack steering system which is the case for the conventional vehicle and leads to a higher maximum η_i. If all of the influencing variables are controllable the sensitivity of the free parameter ΔF_z is very small, which explains why the wheel load distribution is almost the same for both vehicles. However, the sensitivity of ΔF_z is bigger if not all influencing variables are separately actively controllable (e.g. rack steering systems).

7. CONCLUSION

This work presents an approach based on an inverse non-linear vehicle model and a non-linear optimization to investigate vehicles with all useful configurations (actively or passively controlled) for steering, brake/drive, suspension and camber. This leads to the possibility to investigate the vehicle dynamics potentials of all of these configurations and to compare them against each other which may support future decisions concerning these configuration in the early development process of vehicles. While this work presents simulation results for two exemplary different chassis configurations, it is further possible to analyze the effect of actuator failures of these hydraulic or mechatronic systems on the vehicle dynamics for safety and redundancy investigations.

[11] The camber influence is understood as influence on the maximum force. The generation of lateral force due to camber is not reasonable for cars with conventional tyres compared to motorcycles. Nevertheless if unconventional tyres are used (cf. (Ammon, 2004)) lateral force generation due to camber could be reasonable for cars as well.

[12] higher lateral stiffness causes less camber influence.

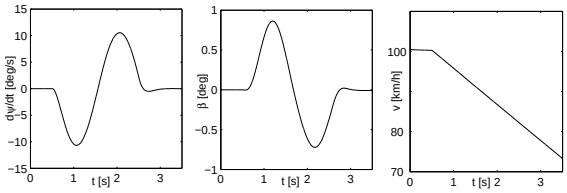

Fig. 5. Plane Motion of the Vehicles

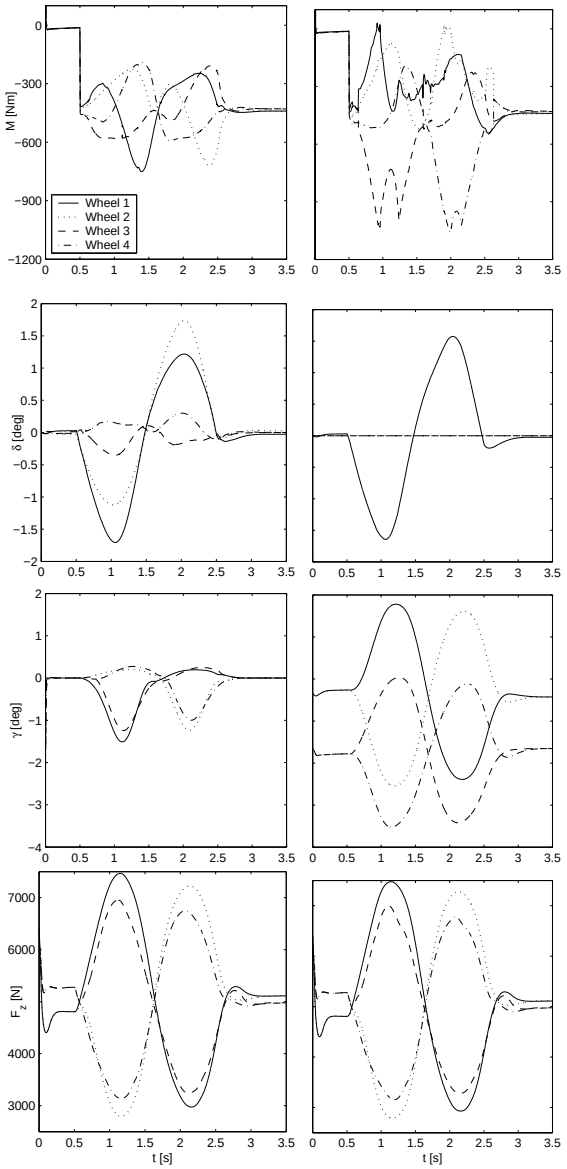

Fig. 6. Influencing Variables of Active (left) and Conventional Vehicle (right)

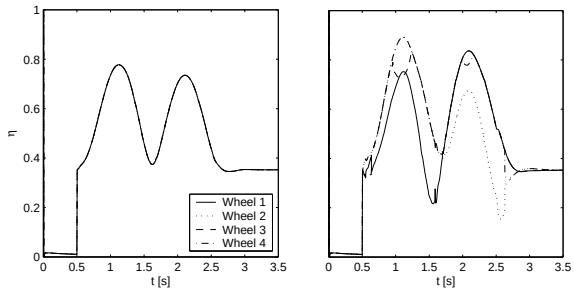

Fig. 7. Adhesion Potential Utilization of Active (left) and Conventional Vehicle (right)

REFERENCES

Ammon, D. (2004). New Perspectives in Vehicle Dynamics the Mechatronic Suspension System of the F400 Carving. In: *Proc. of Technischer Kongress Verband Deutsche Automobilindustrie VDA*.

Andreasson, J. and T. Bünte (2005). Global chassis control based on inverse vehilce dynamics models. Presented at XIX IAVSD World Congress.

Andreasson, J., C. Knobel and T. Bünte (2006). On Road Vehicle Motion Control - striving towards synergy. In: *Proc. of 8th International Symposium on Advanced Vehicle Control AVEC*.

Balas, G. (2003). Flight control law design: An industry perspective. In: *Proc. of European Control Conference*. Vol. 9. pp. 207–226.

Bodson, M. (2002). Evaluation of optimization methods for control allocation. *Jounal of Guidiance, Control and Dynamics*.

Fliess, M., J. Leviene, P. Martin and P. Rouchon (1995). Flatness and Defect of Nonlinear Systems: Introductory Theory and Examples. *Int. J. Control* **61**, 1327–1361.

Hattori, Y., K. Koibuchi and T. Yokoyama (2002). Force and moment control with nonlinear optimum distribution for vehicle dynamics. In: *Proc. of 6th International Symposium on Advanced Vehicle Control AVEC*.

Huang, P.-S. (2004). Regelkonzepte zur Fahrzeugführung unter Einbeziehung der Bedienelementeigenschaften. PhD thesis. TU München.

Ono, E., Y. Hattori, Y. Muragishi and K. Koibuchi (2004). Vehicle dynamics control based on tire grip margin. In: *Proc. of 7th International Symposium on Advanced Vehicle Control AVEC*.

Orend, R. (2004). Steuerung der Fahrzeugbewegung mit minimaler Kraftschlussausnutzung an allen vier Rädern. In: *Proc. of Autoreg*.

Orend, R. (2005). Modelling and control of a vehicle with single-wheel chassis actuators. In: *Proc. of IFAC World Congress*. IFAC.

Pacejka, H. B. (2002). *Tyre and Vehicle Dynamics*. Butterworth-Heinemann. Oxford.

Valášek, M. (2003). Design and control of underactuated and over-actuated mechanical systems - challenges of mechanics and mechatronics. *Vehicle System Dynamics* **40**, 37–50.